ACS OMEGA

Open Access

http://pubs.acs.org/journal/acsodf

Article

In Silico Study of Pyrin and 14-3-3 Protein Modulation During FMF and PAAND

Adrine Paronyan, Nelli Muradyan, Arsen Sargsyan, Vahram Arakelov, Grigor Arakelov,* and Karen Nazaryan

Cite This: *ACS Omega* 2025, 10, 3462−3473

Read Online

ACCESS | Metrics & More | Article Recommendations | Supporting Information

ABSTRACT: Familial Mediterranean fever (FMF) is a genetically determined disease transmitted through autosomal recessive inheritance. Recently, a rare but similar disease to FMF, pyrin-associated autoinflammation with neutrophilic dermatosis (PAAND), has been discovered. PAAND is inherited dominantly and is characterized by neutrophilic dermatosis and recurrent fevers. The cause of the disease is point mutations in the MEFV gene. The pyrin protein is a product of this gene and is one of the main factors in the disease's progression. This paper examines the interaction between pyrin and the 14-3-3 protein and screens for modulators affecting their interaction. Regulating this interaction is crucial for understanding the mechanism of FMF development, specifically the disruption of this complexation, which leads to inflammatory responses. The pyrin−14-3-3 interaction is essential for designing potential drugs since weakening this interaction can result in inflammation. This research of in silico experiments identified low molecular weight chemical compounds that have a modulating effect on the tertiary structures of mutant variations of pyrin and 14-3-3 proteins. Studies have identified modulator molecules that interact with the FMF-associated mutant structure of pyrin (M694I) and 14-3-3τ. The chemical compounds that result from this process can be used as modulators and as a potential new basis for the development of therapeutic drugs.

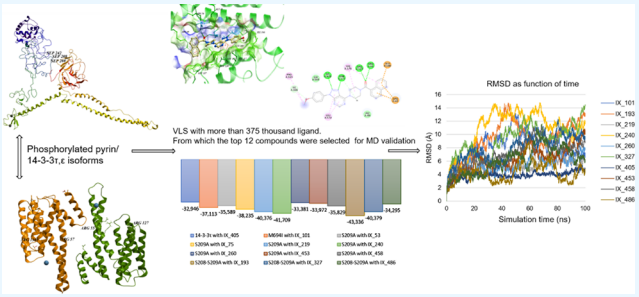

INTRODUCTION

Pyrin is a product of the MEFV gene, whose mutations cause familial Mediterranean fever (FMF) and pyrin-associated autoinflammation with neutrophilic dermatosis (PAAND). FMF and PAAND-associated mutations, toxins, and effectors of various pathogens affect pyrin activation by disrupting the inhibitory interaction of pyrin with the 14-3-3 protein isoforms. Our research is based on the observation of the disruption of the pyrin−14-3-3 complex, which could be the primary cause of pyrin activation and subsequent inflammation during FMF and PAAND.[1] To understand the molecular mechanisms of FMF and PAAND development, we are conducting an in silico study. This study involves the use of small chemical compounds that can modulate the complexation mechanisms of mutated pyrin with 14-3-3 isoforms. This approach is essential for understanding the role of these proteins in disease development. Structural studies of the sites exposed to potential drugs in the interaction regions of these proteins could lead to the discovery of new potential drugs for treating FMF and PAAND. As of 2024, 385 MEFV gene mutations are known, most of which are missense mutations resulting in a single amino acid substitution.[2]

Pyrin consists of 781 amino acid residues and is a positively charged protein with a molecular weight of 86 kDa, 13% of which is lysine and arginine.[3,4] Pyrin expression mainly occurs in cells of the innate immune system, namely granulocytes, eosinophils, monocytes, and dendritic cells.[5] The protein's actual mechanism of action and the cause of its dysfunction due to missense mutations have yet to be elucidated. The result of site-directed mutagenesis indicates the importance of the amino acids S208, S209, and S242 of pyrin for interaction with 14-3-3 isoforms. A single mutation of S208A has been shown to reduce pyrin−14-3-3 interaction; a mutation of S209A does not affect pyrin−14-3-3 interaction; a double mutation of S208−S209A leads to a drastic reduction in pyrin−14-3-3 interaction, and a similar result was obtained with a single mutation of S242A; a triple mutation of S208-S209-S242A also impairs pyrin−14-3-3 interaction.[6]

In the context of this study, 16 pyrin mutations have been studied:

- Mutations affecting pyrin−14-3-3 interaction: S208A, S209A, S242A, S208-S209A, S208-S209- S242A

Received: August 11, 2024
Revised: November 25, 2024
Accepted: December 24, 2024
Published: January 23, 2025

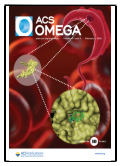

- Mutations localized in the phosphorylation site: S208C and S208T
- PAAND-associated mutations: S242R and E244 K
- FMF-associated mutations: M680I, M694V, M694I, K695R, V726A, A744S, R761H.

14-3-3 isoforms were the first proteins identified as specifically binding phosphoserine/phosphothreonine-containing motifs.[7] 14-3-3 proteins are expressed adaptor proteins that interact with a large number of proteins, mainly to regulate their cellular localization and function.[8] 14-3-3 are involved in cell signaling, regulation of cell cycle development, neurodegenerative processes, apoptosis, carcinogenesis, autophagy, and viral replication. The 14-3-3 proteins consist of seven isoforms (β, γ, ε, η, ζ, σ, and τ/θ) in mammals. There is a high similarity between isoforms 14-3-3, especially in the amphipathic binding groove, while the outer surface carries more variation. The 14-3-3 isoforms differ in the structure of the short variant sites, although they are not products of alternative splicing, and each isoform is encoded by a separate gene.[9] However, further studies revealed specific roles and some differential expression levels in tissues. For example, 14-3-3γ is localized in brain tissue and 14-3-3σ in lymphoid tissue.[1] In many cases, interacting proteins show a clear preference for a particular one of the 7 isoforms of 14-3-3, and in the case of pyrin, two isoforms, ε and τ, have been shown to interact.[10] The 14-3-3 interaction site is represented by the conserved amino acids Arg57, Arg130 in the case of 14-3-3ε (UniProt: P62258) and Arg56, Arg127 in the case of 14-3-3τ (UniProt: P27348). These amino acids interact with the phosphate group of phosphorylated peptides/proteins.

Modulators of protein−protein interactions, low molecular weight chemical compounds, peptides, and larger macromolecules, such as antibodies, were designed as inhibitors or stabilizers of protein complex formation and dynamics.[11] It is worth noting that there are two approaches to drug design by searching for modulators for protein−protein interactions: in the first case, a new compound should be studied on the example of a protein−protein complex, while in the second case, these modulators are studied on the individual proteins, which have not been interacted yet.[12,13] At this stage of our research, virtual screening and search for potential modulators were explicitly performed on individual forms of proteins since the crystallographic structure of the pyrin−14-3-3 complex is not available. The complex-based approach could open perspectives for creating potential therapeutic agents and will be used in our further research.[14]

METHODS

As a full-size native unphosphorylated tertiary structure of pyrin protein, the model previously obtained by the "Laboratory of Computation Modeling of Biological Processes" at the Institute of Molecular Biology of NAS RA was used. Initial models of the tertiary structures of 14-3-3τ and 14-3-3-3ε monomers were obtained using the trRosetta server.[15] After modeling the full-length tertiary structures of 14-3-3τ and 14-3-3ε monomers, protein−protein docking of monomers was performed to obtain the homo- and heterodimers of these 14-3-3 isoforms. The docking was performed using the fast Fourier transform method[16] in the ICM-PRO software package.[17] Molecular modeling of variations in the tertiary structure of mutated pyrin and prediction of the effect of mutations on the stability of the tertiary structure of pyrin will be performed using the ICM-PRO 3.8−7 software package. The Ramachandran plot was generated by ICM-PRO.[17] Molecular dynamics (MD) simulations of native and mutant pyrin, 14-3-3-3ε/ε, 14-3-3-3τ/τ, 14-3-3-3ε/τ and the interactions between them were performed using classical molecular dynamics.

MD simulations were performed using Amber20 software implemented in a graphics processing unit (GPU) using the ff19SB force field.[18] ANTECHAMBER was parametrized with the GAFF force field and the AM1-BCC charge model. All initial structures and the resulting protein−ligand models were solvated in the truncated octahedral box with the TIP3P water model and Na+, Cl− ions at 150 mM.[19] For MD simulations, the chosen step time was 2 fs. The total time in MD simulations in the case of pyrin was 1000 ns; in the case of 14-3-3 proteins, and for all protein−ligand structures, it was 100 structures with a simulated system temperature of 309.75 K at a normal pressure of 1.0 bar. The quality of the model is assessed based on the model's energy or its similarity to the template structure by calculating the standard deviation of the atomic positions of the superimposed proteins.

Distance and RMSD analyses were performed for each MD simulation using the CPPTRAJ program from AmberTools. The distance analysis was based on calculating the distance between the center of mass of the base atoms within a radius of 10 Å. Consequently, the lower the RMSD, the better the model will be. Another important estimation function for identifying the models, precisely the contacts between the protein and the ligand, is a graph of distances over the simulations of the MD. RMSD and distance analysis for all obtained trajectories were performed using the CPPTRAJ program.[20] The cluster analysis method selects the most representative conformational populations obtained directly after the MD simulations. Cluster analysis can be applied in virtual ligand screening studies for a more accurate selection of conformations of protein targets.

TTclust was used for cluster analysis of the obtained trajectories. It is a Python program that uses the MDTraj package in its algorithm to handle the trajectories of MD. The trajectory is aligned with the protein structure, and then the RMSD between all pairs of frames is calculated and stored as a matrix. We used the ward algorithm because it minimizes the variance within clusters, which allows us to obtain clearer clusters.

A dendrogram is generated and plotted to get a graphical representation of the relationship matrix and to see the relationships between all the frames.[21] To create a custom library of modulators, the chemical cartridge MolCart (Molsoft LLC) was used, which contains libraries of chemical compounds from 30 different companies and databases containing information about known modulators of protein−protein interactions.

The final library of protein−protein interaction modulators contained 375558 compounds. Tertiary structures 14-3-3-3τ and 14-3-3-3ε were used to perform 4D docking obtained after MD simulations in which representative structures were selected by clustering. All conformations were superimposed concerning the main conformation, which was the representative structures of 14-3-3-3τ and 14-3-3-3ε, respectively, describing the most common cluster of the 14-3-3-3τ/τ and 14-3-3ε/ε MD trajectories. After analyzing all representative structures of 14-3-3-3τ, 56 amino acids, and in the case of 14-3-3-3ε, 77 amino acids that surrounded the amino acids required for interaction with pyrin were selected as putative ligand interaction sites. The region for 14-3-3-3τ and 14-3-3-3ε containing these sites was further identified, interactions outside of which were not considered.

https://doi.org/10.1021/acsomega.4c07386
ACS Omega 2025, 10, 3462−3473

Also, binding free energies were calculated for each MD simulation system using the Poisson−Boltzmann or generalized Born's method and continuum surface area solvation (MM/PBSA and MM/GBSA) methods and the MMPBSA.py program from the AmberTools package, using 500 frames at equal intervals collected from all MD, with the ionic strength set to 0.150 mM. The frame with the lowest interaction energy was extracted from each MD trajectory to decompose the energies into pairs, which was also done using the MMPBSA.py program.[22]

The online resource ClassyFire (http://classyfire.wishartlab.com/) was used to identify and classify compounds and is a computable chemical taxonomy with a structural ontology that allows the classification of chemical compounds.[23]

The ADMET (Absorption, Distribution, Metabolism, Excretion, and Toxicity) parameter is considered in the analysis of chemical compounds. Data on chemical compounds were extracted using the online SWISS-ADME server.[24]

Toxicity was calculated using the ICM-PRO 3.8-7 software package. The BIOVIA Discovery Studio Visualizer generated a 2D interaction diagram.[25]

RESULTS

Molecular modeling and molecular dynamics simulation of protein structures. Initial models of the tertiary structures of the 14-3-3τ and 14-3-3-3ε monomers were obtained using the trRosetta server. These models were improved and optimized using the ICM-PRO software package. Protein−protein FFT docking in ICM-PRO software was used to model dimer structures. Docking resulted in 10,000 dimer structure models for each case (14-3-3-3τ/τ, 14-3-3-3ε/ε, and 14-3-3-3τ/ε). The models with the lowest interaction energy (14-3-3-3τ/τ- −28.87 kcal/mol, 14-3-3-3ε/ε- −33.18 kcal/mol, 14-3-3τ/ε- −28.32 kcal/mol) and the lowest RMSD value (14-3-3-3τ/τ-4.476 Å, 14-3-3ε/ε-5.426 Å, 14-3-3τ/ε-2.967 Å) as compared to the 6BCR structure were chosen as the best. The Mg ions (1 in each chain) were added as in the compared model. The final dimer models of the 14-3-3-3 isoforms are shown in Figure 1 and Figure 2.

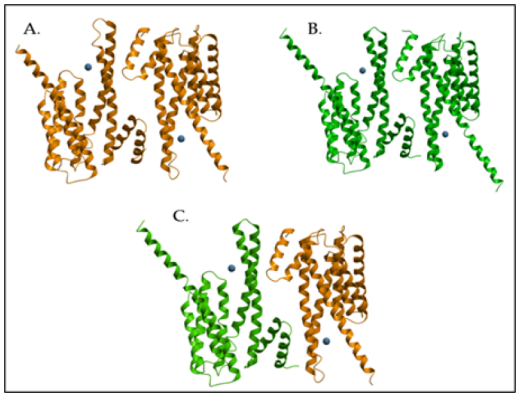

Figure 1. Structures of the dimer models of 14-3-3 isoforms. A: 14-3-3-3τ/τ, B: 14-3-3ε/ε, and C: 14-3-3τ/ε. The 14-3-3-3τ monomers are represented in orange, 14-3-3-3ε, green, and Mg2+ localization in blue. We generated a Ramachandran plot for the resulting models, which shows the conformation of whole protein molecules; each point on the map represents one amino acid residue. The horizontal position of the dot shows the phi angle, and the vertical position shows the psi angle, which is presented in Figure 2.

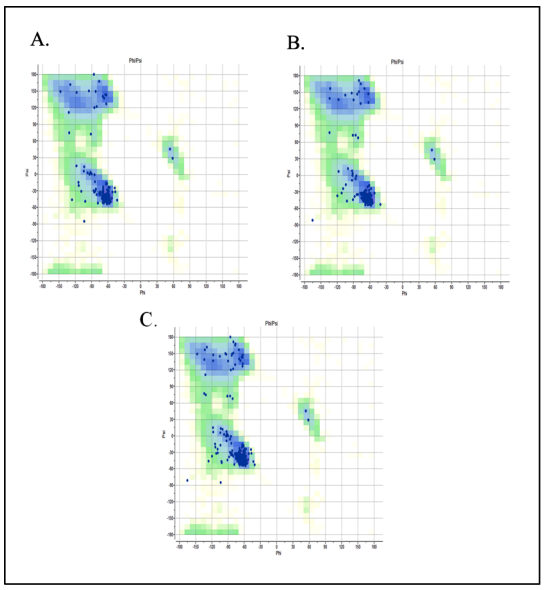

Figure 2. Ramachandran plot of 14-3-3 structures. A. 14-3-3-3τ/τ, B. 14-3-3ε/ε, and C. 14-3-3τ/ε.

Molecular modeling of complete pyrin native and mutated forms tertiary structures was carried out using the ROSETTA 3.8 software package and employed by the RosettaCM algorithm. The amino acid sequence of human pyrin (UniProt ID: O15553) was used for molecular modeling. The structure of the pyrin region, consisting of 214 amino acids (amino acid residues 93−306), which does not have homologues with experimentally studied structures, was predicted using the C-QUARK server. For molecular modeling of the complete native tertiary structure of pyrin, in addition to the known tertiary structures of pyrin domains (PDB ID: 2MPC, 4CG4, 2WL1) and predicted structure of the region consisting of 214 amino acids, 7 homologous structures were also selected (PDB ID: 1FRE, 2DIF, 2EGM, 2JUN, 2YRG, 5JPX, 5OLM). Based on the model of the complete pyrin native tertiary structure thus obtained, its mutated structures were likewise built. Since pyrin binds two Zn2+ ions per subunit, which are its cofactors, we employed induced fit docking of two Zn2+ ions on the pyrin monomer obtained model using the ICM-PRO Explicit Group Docking method (Figure 3). Because, for pyrin−14-3-3 interaction, pyrin has to be phosphorylated, which we perform via ICM-Pro.

To stabilize the resulting models, we performed a classical molecular dynamic of 100 ns duration with a simulation step of 2 fs. Unlike pyrin, 14-3-3 is a rather conservative protein and relatively small in size. As can be seen from the RMSD (Figure 4), the structures are stabilized throughout the dynamics. Dimer complexes obtained by protein−protein docking were used as initial orientations. Figure 3 shows the RMSD oscillations of the dimer 14-3-3 isoforms main chain during the molecular dynamics simulation.

Cluster analysis was implemented after molecular dynamics simulations of the isoform 14-3-3 dimers. To cluster the trajectories of all 14-3-3 systems studied (5000 frames each), Cα atoms were used for superimposition coordinates, and all atoms except hydrogen were used for RMSD calculations. Molecular dynamics modeling was done for both native and mutated variations of pyrin. Models obtained by optimization in ICM were used as initial orientations. The simulation time for all

https://doi.org/10.1021/acsomega.4c07386
ACS Omega 2025, 10, 3462−3473

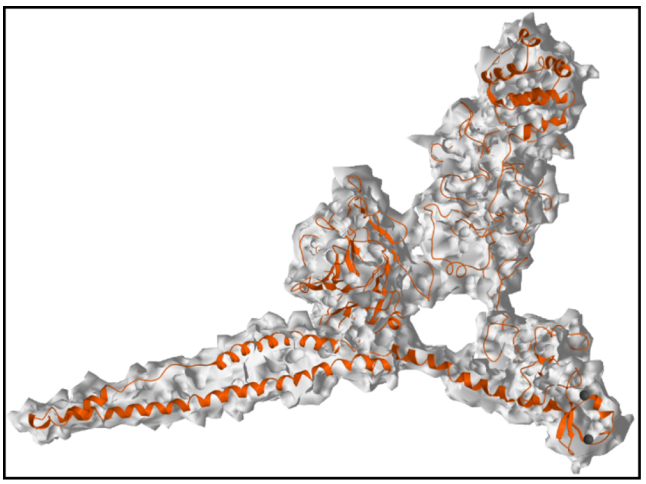

Figure 3. Structures of the native pyrin.

systems was 1000 ns (each) with a simulation step of 2 fs. Figure 5 shows the RMSD variations of the main chain tertiary structures of the native and mutated variations of pyrin throughout the molecular dynamics simulations. Based on the RMSD values, we can conclude that the structures are relatively stabilized.

Since pyrin is sufficiently large (781 amino acid residues) and contains disorder regions, the obtained structures can be considered successful. It should also be noted that the fluctuations are within the acceptable norm of 2 Å. We received a Ramachandran plot for all mutated pyrin structures (Figures S1−S17).

4D docking and virtual screening of proteins with a compound library. After modeling the molecular dynamics of the native and mutated variations of pyrin, a cluster analysis was performed. To cluster the trajectories of all studied pyrin systems (50,000 frames each), Cα atoms were used for superimposition coordinates, and all atoms except hydrogen were used for RMSD calculations. Every fifth frame from the trajectories (10,000 frames each) was subject to cluster analysis. The cluster analysis identified clusters whose representative structures were used. Initially, 4D docking and virtual screening were performed for 14-3-3τ. Of 375558 compounds, 679 showed promising results with an ICM docking score equal to or less than −32, considered the minimum acceptable docking score in the ICM-PRO program. For these compounds, the virtual screening and 4D docking experiments were independently repeated 10 times after the compounds that corresponded to the acceptable docking score resulting from 11 independent virtual screening and 4D docking experiments were selected.

Only the compounds that had statistical validity in 100% of experiments performed have been selected, and only one best compound, IX_405, has been chosen based on the average docking score (−32,946) and localization in the previously selected interaction site 14-3-3τ with pyrin.

Compound IX_405 interacts with an energy of −9.75 kcal/mol, forming 4 hydrogen bonds in the interaction site 14-3-3τ with pyrin. Of all the studied interaction sites of IX_405 with 14-3-3τ, R56, and R127, essential amino acids for interacting 14-3-3τ with pyrin should be highlighted (Figure 6).

In the case of FMF-associated mutations, only the pyrin M694I structure showed promising results with one best compound, IX_101, which had an average docking score of −37.113 and was localized in the previously selected interaction site of pyrin with isoforms 14-3-3 (Figure 7).

In the case of the mutated S209A pyrin structure, 7 compounds, IX_53, IX_75, IX_219, IX_240, IX_260, IX_453, and IX_458, were selected and had docking score averages of −35.589, −38.235, −40.376, −41.709, −33.381, −33.972, and −35.829 (Figures 7−89).

IX_53 interacts with an energy of −9.8 kcal/mol, forming 6 hydrogen bonds in the interaction site of the mutated form of pyrin S209A. Of all the interaction sites studied for IX_53 with pyrin, the E244 should be highlighted because this amino acid is essential for the pyrin−14-3-3 interaction.

IX_75 interacts with an energy of −11.27 kcal/mol, forming 2 hydrogen bonds at the pyrin−14-3-3 interaction site. Among all the interaction sites of IX_75 with the mutated form of pyrin S209A studied, the E244 should be highlighted as an essential amino acid for the interaction of pyrin with 14-3-3.

IX_240 interacts with an energy of −12.67 kcal/mol, forming 4 hydrogen bonds in the pyrin c 14-3-3 interaction site. This compound interacts with the E244 mutated form of pyrin S209A, which is essential for the interaction of pyrin with 14-3-3.

The protein interacts with the ligand, and it is necessary to understand which electrons are involved in forming covalent or noncovalent bonding. This characteristic is described by π-alkyl

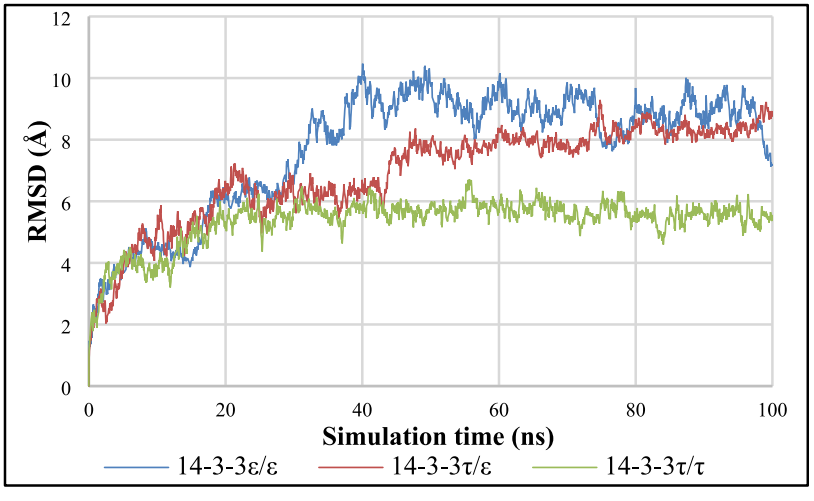

Figure 4. RMSD of 14-3-3ε/ε, 14-3-3τ/ε, and 14-3-3-3τ/τ.

https://doi.org/10.1021/acsomega.4c07386
ACS Omega 2025, 10, 3462−3473

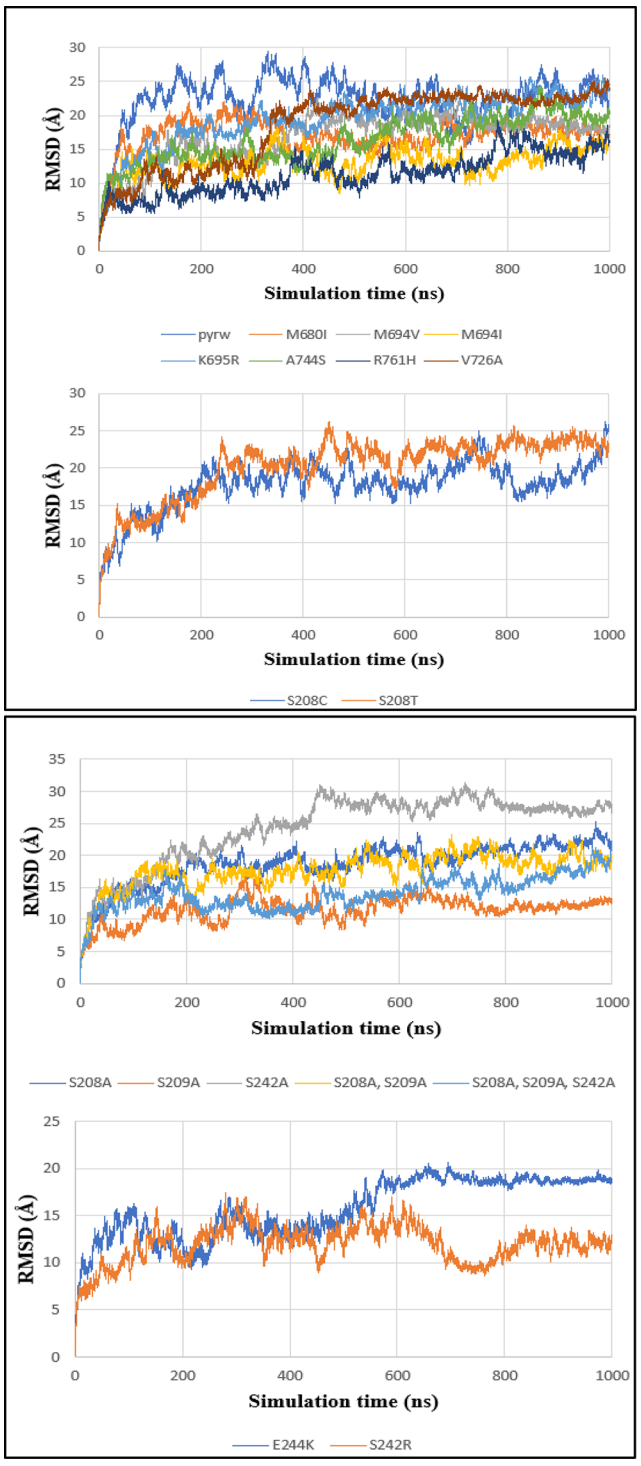

Figure 5. RMSD of native and mutated pyrin variations.The results showed that the average RMSD for 14-3-3ε/ε was 7.74 Å, 14-3-3τ/ε was 6.92 Å, and 14-3-3-3τ/τ was 5.34 Å; in total, the average RMSD for the resulting 14-3-3 structures were 6.67 Å. In the case of the mutant variations of pyrin the mean RMSD values were: S208A 18.69 Å, S209A 11.52 Å, S242A 24.33 Å, S208A/S209A 17.66 Å, S208A/S209A/242A 14.04 Å, S208C 17.76 Å, S208T 20.15 Å, E244 K 15 72 Å, S242R 11.95 Å, M680I 17.12 Å, M694 V 16.88 Å, M694I 13.11 Å, K695R 19.34 Å, A744S 16.36 Å, R761H 11.32 Å, V726A 18.44 Å, and for the native pyrin structure the average RMSD was 22.29 Å. To summarize, the average RMSD for the above pyrin systems was 16.87 Å, and for 14-3-3 was 6.66 Å.

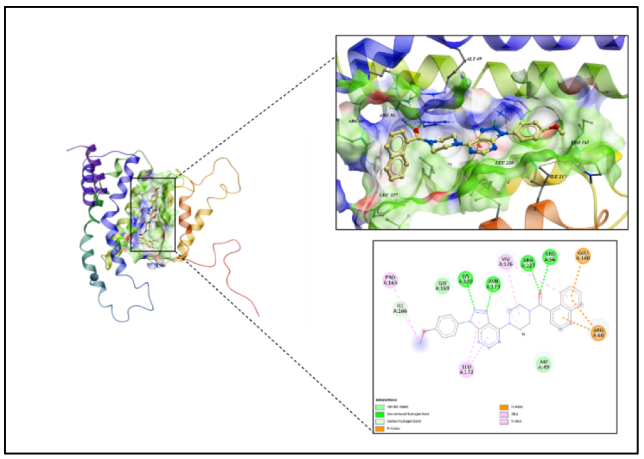

Figure 6. Interaction of 14-3-3τ with IX_405. The ligand localization in the 14-3-3-3τ interaction pocket and a 2D diagram of the interaction sites are shown.

(π-electron cloud interaction between an aromatic group and the electron group of any alkyl group) and π-π interactions (π-electron cloud interaction between two aromatic groups).

Also, we must mention the vital interaction between hydrogen bonds and van der Waals. These interactions determine the formation of the spatial structure of biological macromolecules. All these connections are shown in Figures 6−10 in the 2D diagram of the interaction side.

IX_219 interacts with an energy of −11.39 kcal/mol, forming 4 hydrogen bonds in the pyrin c 14-3-3 interaction site. IX_219 interacts with the E244 mutated form of pyrin S209A, which is essential for the interaction of pyrin with 14-3-3.

IX_260 interacts with an energy of −8.52 kcal/mol, forming 4 hydrogen bonds in the pyrin−14-3-3 interaction site. Of all the interaction sites studied for IX_260 of the mutated form of S209A pyrin, E244 is of particular note as an essential amino acid for the interaction of pyrin−14-3-3.

IX_453 interacts with an energy of −9.65 kcal/mol, forming 4 hydrogen bonds in the interaction site of pyrin c 14-3-3. Of all the interaction sites studied for IX_453 with the mutated form of pyrin S209A, E244, which is an essential amino acid for the interaction of pyrin with 14-3-3, should be highlighted.

IX_458 interacts with an energy of −10.28 kcal/mol, forming 2 hydrogen bonds in the pyrin c 14-3-3 interaction site. IX_458 interacts with the amino acid E244 of the mutated form of pyrin S209A, an essential amino acid for the interaction site of 14-3-3 with 14-3-3.

IX_193 interacts with an energy of −18.26 kcal/mol, forming 4 hydrogen bonds in the interaction site of pyrin with 14-3-3. Of all the studied interaction sites of IX_193 with the mutated form of pyrin S208-S209A, the A209, an essential amino acid for interacting with 14-3-3, should be highlighted.

IX_327 interacts with an energy of −16.74 kcal/mol, forms 4 hydrogen bonds in the interaction site of pyrin c 14-3-3, and shows interaction with A209, which is a necessary amino acid for interaction with 14-3-3.

IX_486 interacts with an energy of −11.08 kcal/mol and forms 3 hydrogen bonds in the interaction site of pyrin−14-3-3. Of all the studied interaction sites of IX_486 with the mutated form of pyrin S208-S209A, the A209 is included in the interaction site 14-3-3. It is an essential amino acid for the interaction of pyrin with 14-3-3 (Figure 10) highlighted.

https://doi.org/10.1021/acsomega.4c07386
ACS Omega 2025, 10, 3462−3473

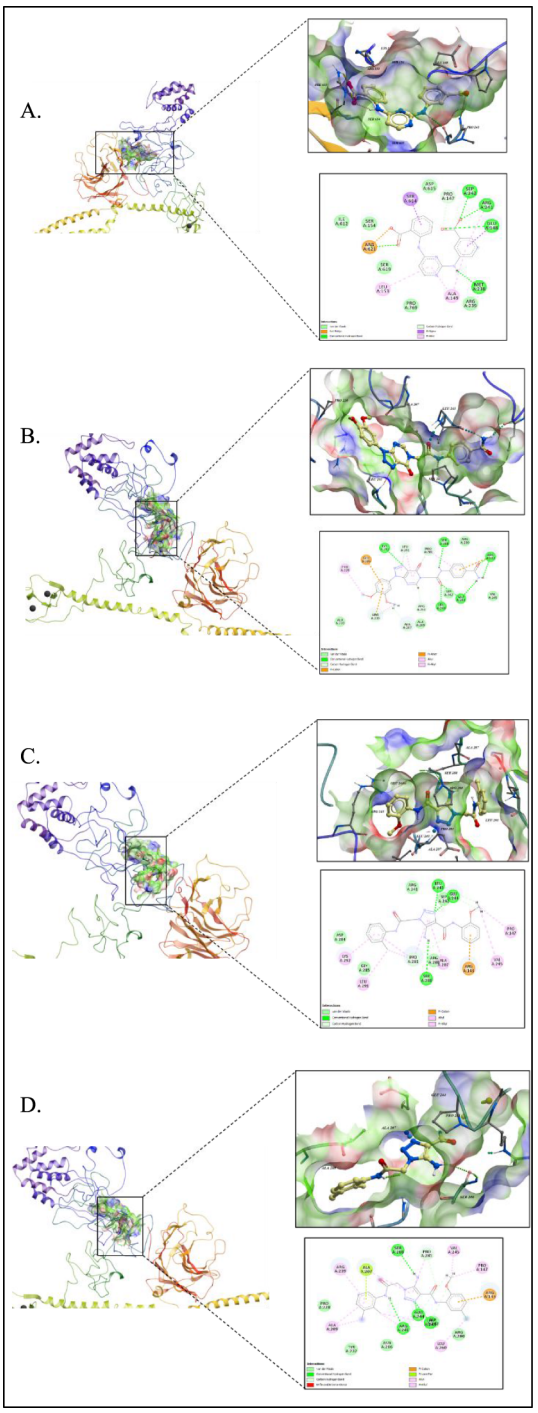

Figure 7. Interaction of the mutated form of M694I and S209A pyrin. A: M694I with IX_101. B: S209A with IX_53. C: S209A with IX_75. D: S209A with IX_240. The localization of the ligand in the pyrin interaction pocket and a 2D diagram of the interaction sites are shown.

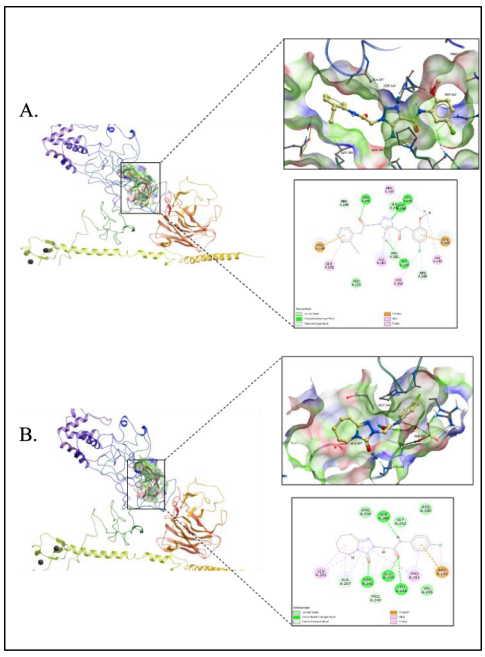

Figure 8. Interaction of the mutated form of S209A pyrin. A: S209A with IX_219, B: S209A with IX_260. The ligand's localization in the pyrin's interaction pocket and a 2D diagram of the interaction sites are shown.

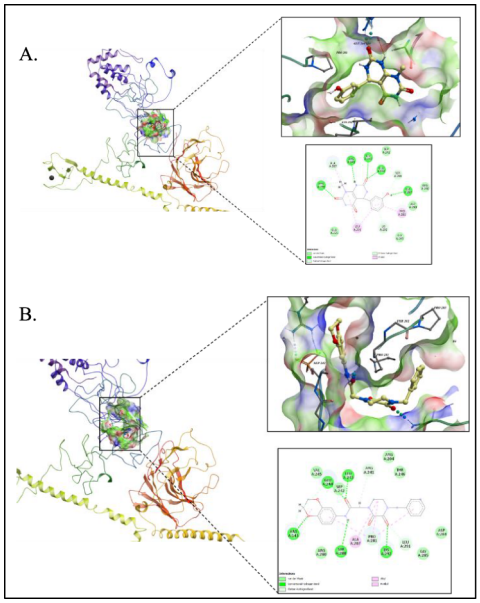

Figure 9. Interaction of the mutated form of S209A pyrin. A: S209A with IX_453, B: S209A with IX_458. The ligand's localization in the pyrin's interaction pocket and a 2D diagram of the interaction sites are shown.

The docking score of selected compounds in the ICM-Pro software package is presented in Scheme 1.

In silico experiments such as protein tertiary structure modeling, molecular dynamics simulation, molecular docking, and virtual ligand screening have identified low molecular weight chemical compounds with modulating effects on tertiary structures of mutated variations of pyrin and 14-3-3τ. In our study, we found modulator molecules that interact with both FMF-associated mutated pyrin (M694I) and mutated tertiary variations directly in the interaction site (S209A and S208-209A) with 14-3-3 isoforms (Table 1).

We performed the MD simulations of ligand structure with protein for 100 ns each. After that, we used the method MMPBSA/MMGBSA to calculate ΔG (Gibbs free energy) and plot distances. Computationally efficient techniques like MMGBSA and MMPBSA are prevalent for estimating the energy of complex formations. These methods calculate the energies of the entire complex and its constituents from the MD

https://doi.org/10.1021/acsomega.4c07386
ACS Omega 2025, 10, 3462−3473

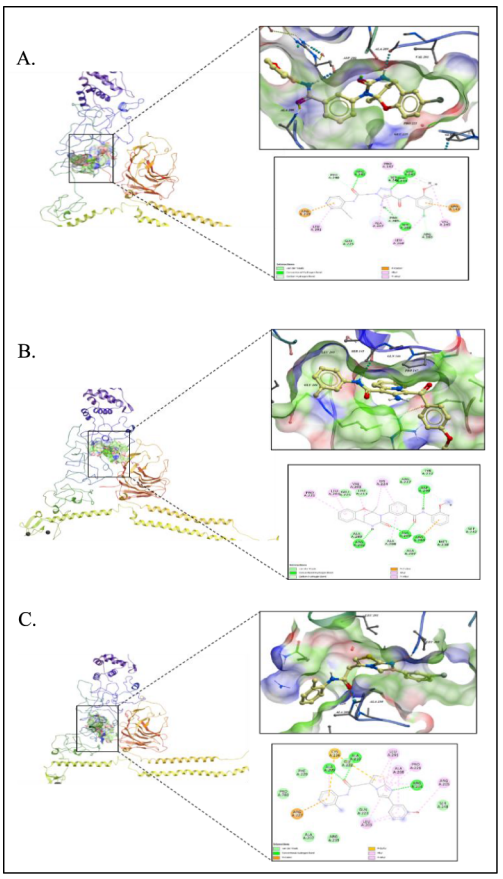

Figure 10. Interaction of the mutated form of S208-S209A pyrin. A: S208-S209A with IX_193, B: S208-S209A with IX_327, C: S208-S209A with IX_486. The localization of the ligand in the pyrin interaction pocket and a 2D diagram of the interaction sites are shown.

Scheme 1. Top Structures by Docking Score

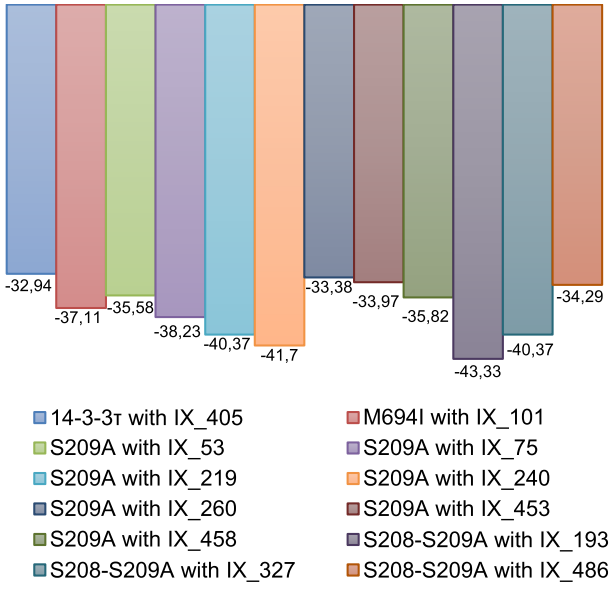

modeling for each molecular conformation. A continuous medium replaces the solvent with a given dielectric permittivity. Table 2 shows the results obtained for MMGBSA and MMPBSA.

Table 1. Selected Modulators of Pyrin and 14-3-3 Interaction

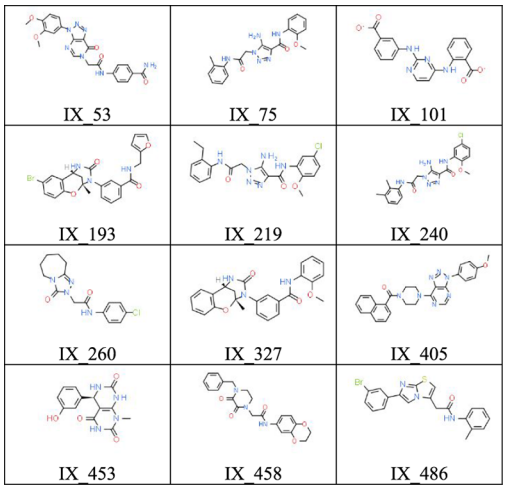

Table 2. MMGBSA and MMPBSA of Selected Compounds

Structure	MMPBSA (kcal/mol)	MMGBSA (kcal/mol)
S209A IX_53	−21.9496	−23.2280
S209A IX_75	−22.6470	−52.3083
S209A IX_219	−33.1411	−33.1502
S209A IX_240	−29.9497	−38.2427
S209A IX_260	−18.4526	−21.5323
S209A IX_453	−22.2913	−28.8549
S209A IX_458	−33.1792	−33.0161
M694I IX_101	−32.4251	−32.4251
S208-S209A IX_193	−27.6750	−43.2220
S208-S209A IX_327	−34.4408	−48.9849
S208-S209A IX_486	−33.4341	−41.3134
14-3-3τ IX_405	−18.7300	−0.3619

We note that all compounds showed promising results of binding energies. Only in the case of the compound IX_405 MMPBSA showed slightly low binding energy. Distance analysis allows us to measure the interatomic distance between the protein and the selected ligand. As a result, we can see how the contact between the protein and the ligand changes over the simulations of the MD. This analysis was performed for all selected structures and presented inFigures S18−S29. The data shows that the ligands interact with the proteins, and the graph indicator is in the normal range in all cases. The average RMSD for structures with ligands interacting with pyrin was on average IX_101 8.16 Å, IX_193 9.29 Å, IX_219 5.54 Å, IX_240 10.77 Å, IX_260 5.46 Å, IX_327 9.17 Å, IX_453 6.39 Å, IX_458 7.11 Å, IX_486 4.27 Å, IX_53 7.88 Å, IX_75 6.08 Å. For 14-3-3, the only interacting ligand IX_405 interacted with an average RMSD of 3.89 Å. That is, the average RMSD for all systems was 7.01 Å. Figure 11 shows the RMSD plots for ligand-protein structures throughout the dynamics.

The system is considered balanced and stabilized when it receives low RMSD levels with constant fluctuations for the entire simulation, and only higher fluctuations indicate low stability. Strongly deviated RMSD plots can also indicate major conformational transitions in the protein to obtain a stable conformation with the ligand. Based on Figure 11, which shows all RMSD plots for protein−ligand systems, we can note that the structures are relatively stable. By the following analysis, we calculated the interaction distances of the protein with the ligand, the graph of which is shown in Figure 12.

https://doi.org/10.1021/acsomega.4c07386
ACS Omega 2025, 10, 3462−3473

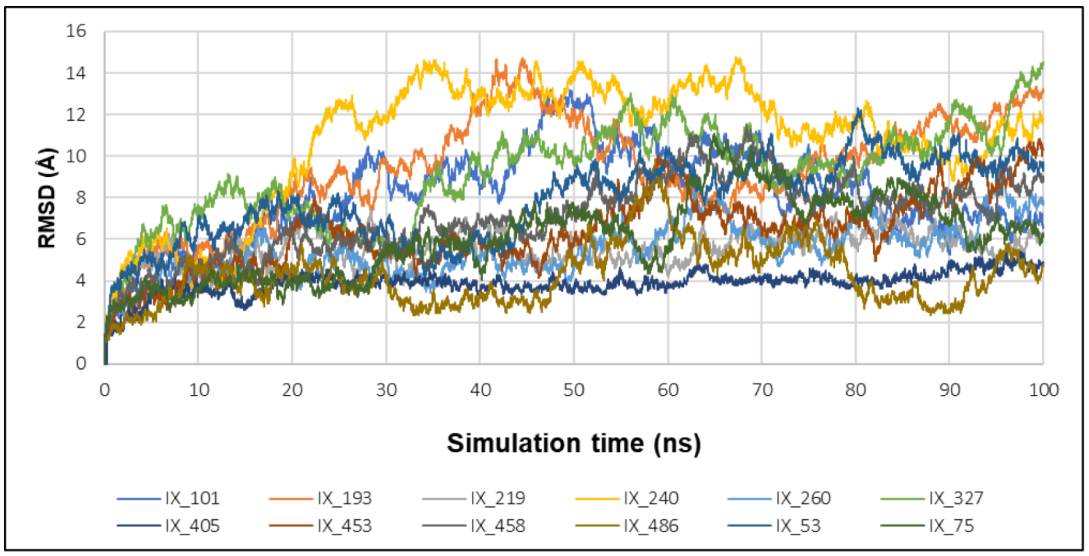

Figure 11. During the MD simulation, the RMSD trajectory of protein−ligand complex.

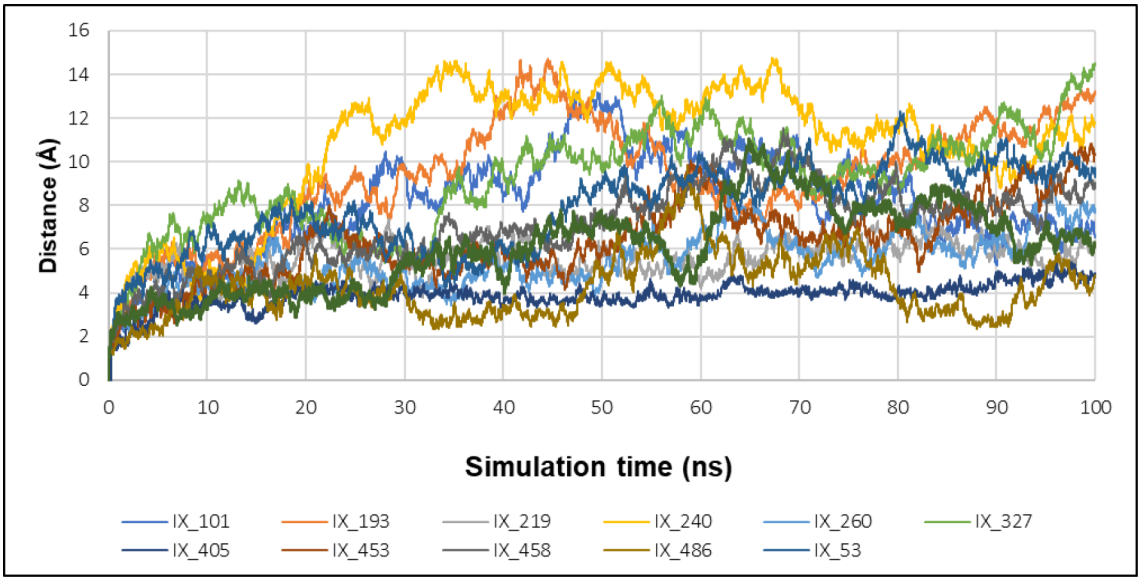

Figure 12. Interaction distance between the proteins and ligands.

Distance analysis allows us to measure the distance between two atoms. This analysis is performed based on the MD trajectory, which can be visualized with a graph, and their fluctuations are noted. Such information is one of the most important for revealing the stability of the structure and the interaction between the protein and the ligand. Structure IX_405 showed relatively poor results and thus is not included in the graph shown in Figure 12. The high fluctuations provide information that the structure is unstable and, therefore, weakly interacts with protein 14−3−3. Namely, the connection with the protein is broken at 25 ns. This compound was not considered in further analyses. Compound IX_53 also shows some fluctuations. However, after visualization of the MD trajectory, we noticed that this structure does not go beyond the interaction package with the protein and only has some fluctuations, which can be considered within the normal range. Decomposition analysis was performed to identify the binding energy of each amino acid in a protein with ligand, shown in Figure 13 for IX_405 and other of the selected structures, as presented in the Supporting Information in Figures S30−S40. Per-residue decomposition is an analytical method used to evaluate the contribution of individual protein amino acid residues and ligand atoms to the total binding energy of a protein−ligand complex.

This method identifies key amino acid residues and interactions that play a critical role in binding and provides a detailed view of the molecular interactions in protein−ligand complexes, significantly contributing to the rational design of new therapeutics. In the graphs below, we have filtered out those amino acids that are key in terms of interaction sites and have the best binding energies.

Chemoinformatic Analysis of Selected Compounds. We performed a taxonomic analysis that yielded a division into two superclasses, benzoids (IX_101, IX_53, IX_75, IX_219, IX_240, IX_260, IX_327) and organoheterocyclic compounds (IX_453, IX_458, IX_193, IX_486). It could be divided into classes: benzene and substituted derivatives (IX_101), benzoic acids and derivatives (IX_53), anilides (IX_75, IX_219,

https://doi.org/10.1021/acsomega.4c07386
ACS Omega 2025, 10, 3462−3473

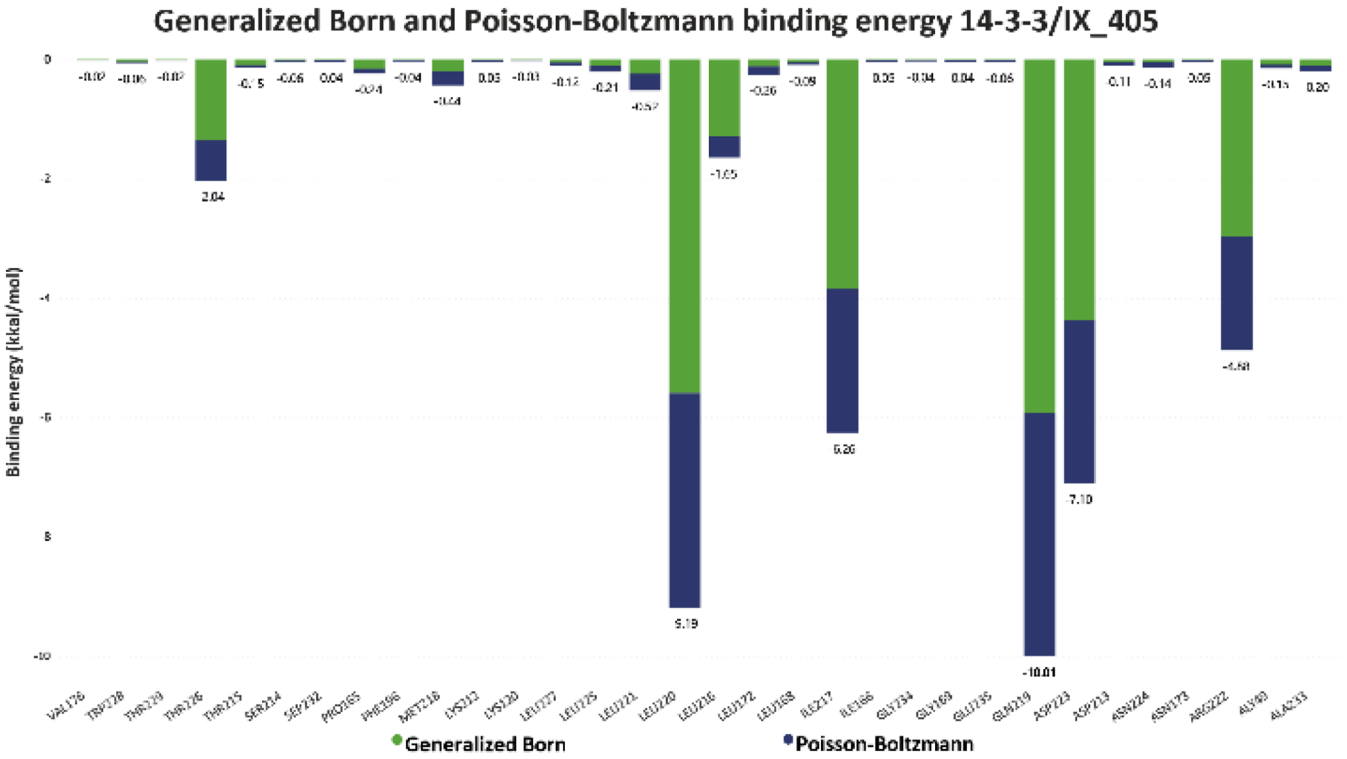

Figure 13. Decomposition graphic 14−3−3τ with IX_405.

Scheme 2. Values of Molecular Weight, TPSA, and Molecular Refraction

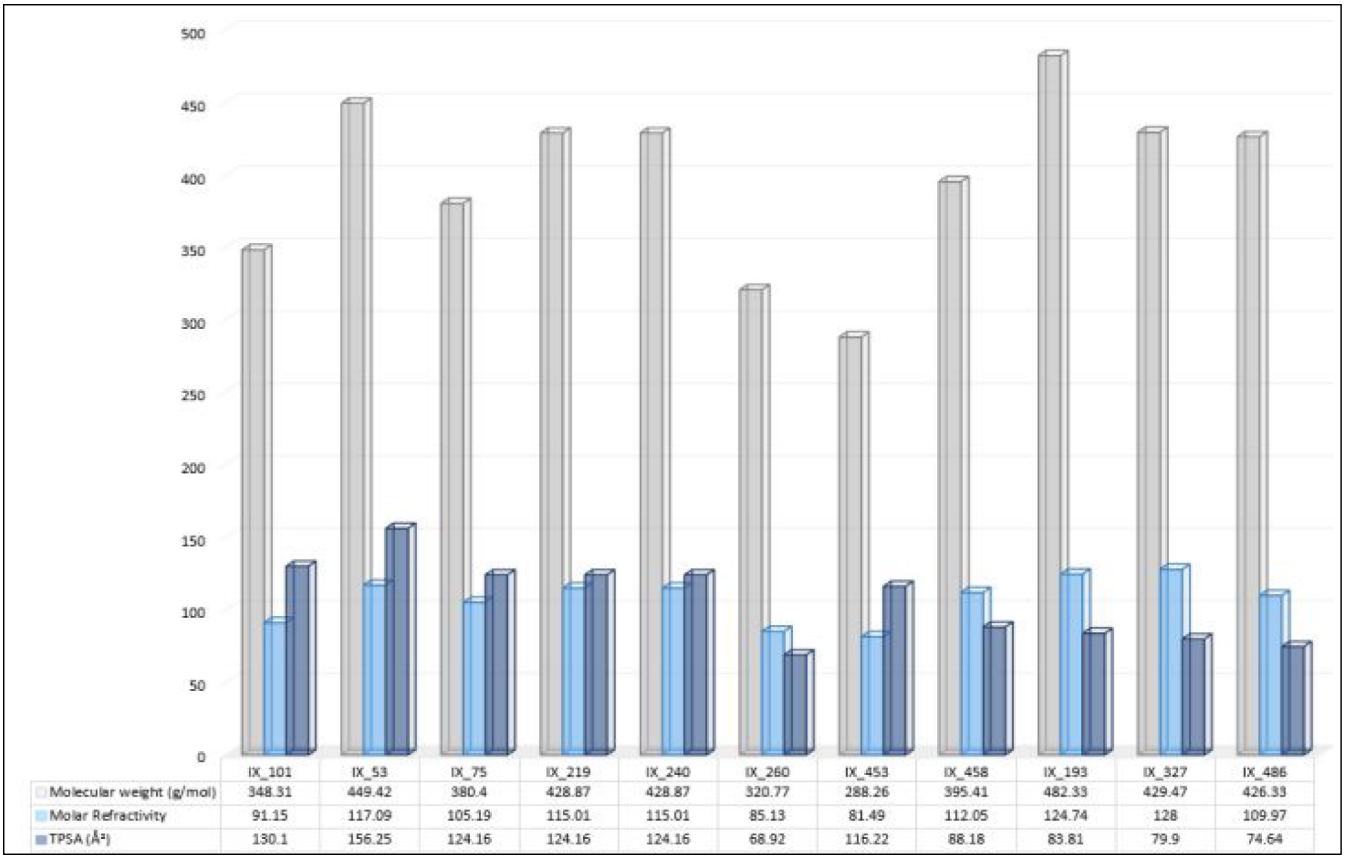

	IX_101	IX_53	IX_75	IX_219	IX_240	IX_260	IX_453	IX_458	IX_193	IX_327	IX_486
Molecular weight (g/mol)	348.31	449.42	380.4	428.87	428.87	320.77	288.26	395.41	482.33	429.47	426.33
Molar Refractivity	91.15	117.09	105.19	115.01	115.01	85.13	81.49	112.05	124.74	128	109.97
TPSA (Å²)	130.1	156.25	124.16	124.16	124.16	68.92	116.22	88.18	83.81	79.9	74.64

IX_240, IX_260, IX_327), organoheterocyclic compounds-pyridines and derivatives (IX_453), piperazines (IX_458), benzopyrans (IX_193) imidazoles (IX_486). ADMET parameters include molecular weight, which should range from 180 to 480, while poor absorption is observed at a molecular weight greater than 500. The topological polar surface area (TPSA) is

https://doi.org/10.1021/acsomega.4c07386
ACS Omega 2025, 10, 3462−3473

Scheme 3. Values of the Number of Heavy Atoms, the Number of Acceptor Atoms for H-bonds, the Number of Donor Atoms for H-bonds, the Number of rotating Bonds, and the Lipophilicity of logP

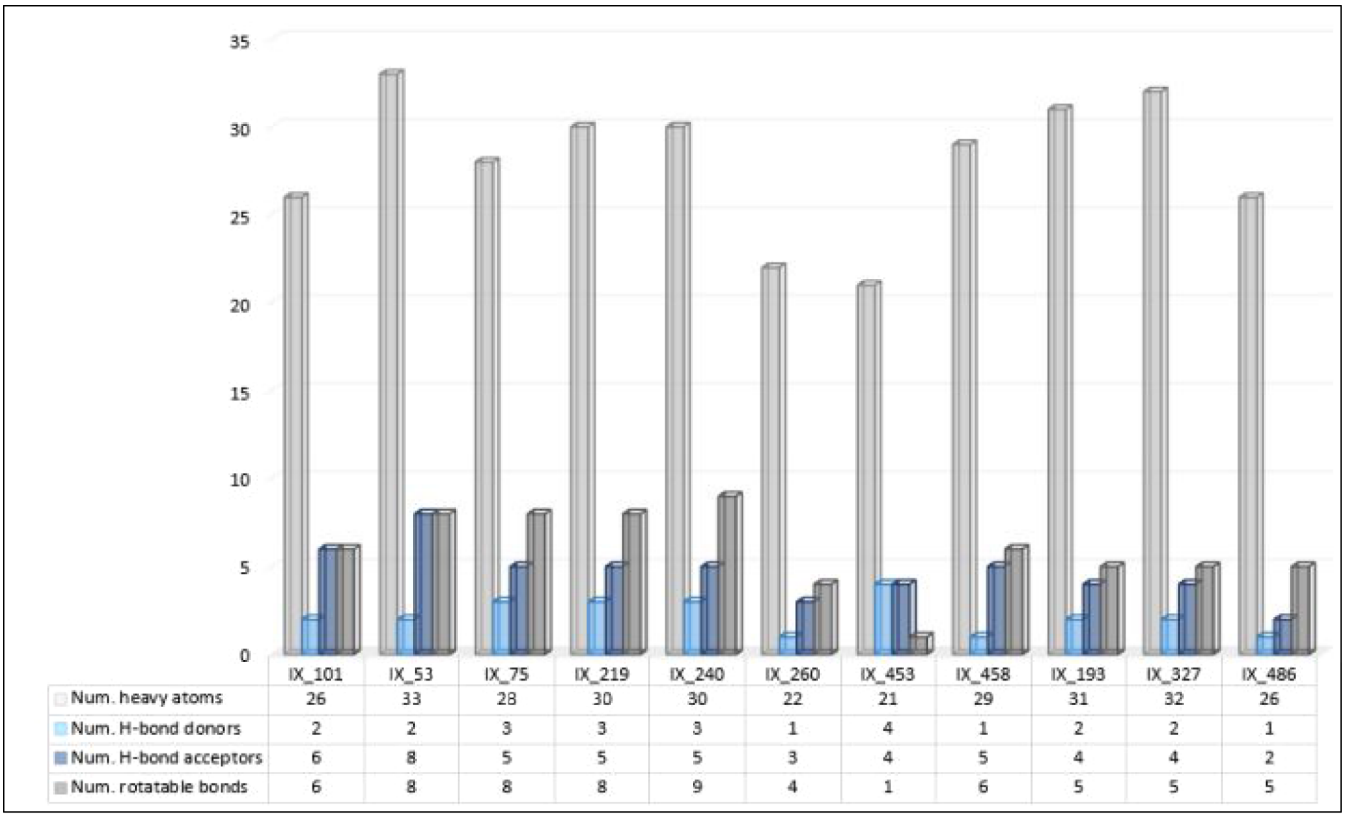

	IX_101	IX_53	IX_75	IX_219	IX_240	IX_260	IX_453	IX_458	IX_193	IX_327	IX_486
Num. heavy atoms	26	33	28	30	30	22	21	29	31	32	26
Num. H-bond donors	2	2	3	3	3	1	4	1	2	2	1
Num. H-bond acceptors	6	8	5	5	5	3	4	5	4	4	2
Num. rotatable bonds	6	8	8	8	9	4	1	6	5	5	5

also considered a substantial property. It is a helpful descriptor in many models and rules to quickly assess some properties of ADMET, especially concerning crossing biological barriers such as absorption and access to the brain. The TPSA range should be between 20 and 130 Å.[26] The molar refraction represents the actual molecules' volume and should be between 40 and 130.[27] Scheme 2 shows the parameters listed above.

The diagram shows that compound IX_458 does not correspond to the molecular weight parameter, and TPSA does not correspond to compound IX_101. The basic properties of the physicochemical parameters are also considered to be such as the number of heavy atoms in the aromatic system, the number of acceptor atoms for H-bonds (<10), the number of hydrogen bond donors (<5), the number of rotating bonds (<15), lipophilicity (LogPo/w).[28]

All compounds showed promising results for the selected parameters shown in Scheme 3.

Essential parameters in selecting potential drugs are Lipinski's rule of five, Muguet's rule proposed by Bayer Pharmaceuticals, and Weber's filter.[29] Based on those compounds, only IX_53 and IX_486 did not fit the specified regulations and criteria.

The last criterion included in ADMET is the toxicity characteristic Table 3.

Table 3. Toxicity Analysis Results Obtained by ICM-Pro[ab]

Compound	Tox Name	Tox Score
IX_101		0
IX_75		0
IX_219		0
IX_240		0
IX_260	Hydrazone	0.2357
IX_453		0
IX_458		0
IX_193		0
IX_327		0

[a]The final criterion is toxicity, which was done. [b]Based on this Table 3, we can see that only compound IX_260 has apparent toxicity.

DISCUSSION

The protein−protein interaction between pyrin and the 14−3−3 protein is of significant interest in the fields of structural bioinformatics, especially in the context of the development of new therapeutics. Modulation of the interaction between pyrin and 14−3−3 may open new therapeutic options for treating diseases associated with pyrin dysfunction such as FMF and PAAND. The importance of these protein interactions is, that when complexed with 14−3−3, pyrin remains inactivated and does not participate in the formation of an active inflammasome.[30]

Research on protein−protein interactions and the search for their modulators is an actively developing area. For example, the interaction between p53 and MDM2 is a well-studied target for anticancer drug development. Nutlin-3 and Etipladen and its analogs have been shown to effectively inhibit the p53-MDM2 interaction, activating the p53 pathway and inducing apoptosis in tumor cells.[31,32] In another study, inhibitors of BCL-2 and BAX interaction, such as ABT-737 and its analogs, demonstrated the ability to induce apoptosis in leukemia cells and other types of cancer.[33,34] These studies support the importance of modulating protein−protein interactions in the development of new therapeutic approaches.

https://doi.org/10.1021/acsomega.4c07386
ACS Omega 2025, 10, 3462−3473

Using bioinformatics approaches and, in particular, a virtual screening method of searching for a potential modulator that could stabilize protein−protein interactions by reviewing and simulating on individual proteins rather than on the complexes themselves, taking into account the necessary amino acid residues that are key for 14−3−3 and pyrin interaction. In addition to the binding sites and energy bonds after virtual screening, the ICM scoring function was also used, which indicates the interaction of the protein with the ligand, where the minimum threshold is considered to be −32 and less. All selected compounds show −32 or less for all 10 replicates of VLS as well as interaction with important amino acids for protein−protein interaction for this research of pyrin/14−3−3. Specifically, in the case of 14−3−3ε, we used Arg 57 and Arg 130 (UniProt ID: P62258) as significant, and in the case of 14−3−3τ, Arg 56 and Arg 127 (UniProt ID: P27348) played key roles in the protein−protein interaction. A recently published study also confirmed the right selection of the use of active interaction sites.[35] Thus, the authors note the importance of amino acids Ser 208 and Ser 242 in the case of pyrin 14−3−3 binding, but we also considered amino acid Ser 209[1,6].

The results of the virtual screening showed that several compounds have potentially high affinity and specificity for the target complex. Based on the search we selected only those ligands that formed an interaction with the required amino acid residues. The important method that we used for searching the binding affinity between protein and ligands was MMGBSA/MMBSA, which showed good results in interaction energy. The analyses of the distances, decomposition, and RMSD which were completed also showed good results in our experiments. Among them, compounds were identified which showed the best results in terms of binding parameters and stability of the complex. These modulators represent that can modulate inflammatory processes through the regulation of pyrin-14−3−3 interactions.

As a result of using this, as well as the number of other selection criteria and repeating the screening experiments 10 times, only 12 compounds were selected to search for ligands. Their chemical characteristics and accepted parameters, such as ADMET, Lipinski, Muguet, and Weber, must be considered when selecting potential drugs. After analysis which we performed based on distance results such as RMSD and MMGBSA/MMBSA out of the initial library of compounds, which amounted to more than 375 thousand ligands, only 8 showed promising results in silico experiments. Taking into a count theoretical basics for our experiments these can be used as a potential therapeutic agent. The identified modulator molecules could theoretically serve as the basis for the creation of fundamentally new therapeutic drugs that directly affect FMF and/or PAAND due to their direct interaction with the mutated pyrin-14−3−3 complex and their modulating effect on it. Thus, confirms the importance of the structural approach in the development of new drugs and opens prospects for further study of the modulation of protein−protein interactions in clinical settings.

■ ASSOCIATED CONTENT

Supporting Information

The Supporting Information is available free of charge at https://pubs.acs.org/doi/10.1021/acsomega.4c07386.

Ramachandra plot of native phosphorylated and mutated pyrin structures (Figures S1−S17); distance graphics of pyrin and 14-3-3τ with selected compounds (Figures S18−S29); decomposition graphic pyrin with selected compounds (Figures S30−S40); table of Cluster results for 14-3-3 dimers, native phosphorylated and mutated pyrin (Table S1) (PDF)

■ AUTHOR INFORMATION

Corresponding Author

Grigor Arakelov − *Institute of Molecular Biology of the National Academy of Sciences of the Republic of Armenia (NAS RA), Yerevan 0014, Armenia; Russian-Armenian (Slavonic) University, Yerevan 0051, Armenia; International Scientific-Educational Center of NAS RA, Yerevan 0019, Armenia;* orcid.org/0000-0003-3697-4512; Email: g_arakelov@mb.sci.am

Authors

Adrine Paronyan − *Institute of Molecular Biology of the National Academy of Sciences of the Republic of Armenia (NAS RA), Yerevan 0014, Armenia; Russian-Armenian (Slavonic) University, Yerevan 0051, Armenia;* orcid.org/0009-0005-9315-6606

Nelli Muradyan − *Institute of Molecular Biology of the National Academy of Sciences of the Republic of Armenia (NAS RA), Yerevan 0014, Armenia; International Scientific-Educational Center of NAS RA, Yerevan 0019, Armenia*

Arsen Sargsyan − *Institute of Molecular Biology of the National Academy of Sciences of the Republic of Armenia (NAS RA), Yerevan 0014, Armenia; Russian-Armenian (Slavonic) University, Yerevan 0051, Armenia*

Vahram Arakelov − *Institute of Molecular Biology of the National Academy of Sciences of the Republic of Armenia (NAS RA), Yerevan 0014, Armenia*

Karen Nazaryan − *Institute of Molecular Biology of the National Academy of Sciences of the Republic of Armenia (NAS RA), Yerevan 0014, Armenia; Russian-Armenian (Slavonic) University, Yerevan 0051, Armenia*

Complete contact information is available at: https://pubs.acs.org/10.1021/acsomega.4c07386

Funding

The work was supported by the Science Committee of RA, in the framework of the research project No 21AG-1F057 and Foundation Armenia (Switzerland).

Notes

The authors declare no competing financial interest.

■ ACKNOWLEDGMENTS

We also thank the Joint Institute for Nuclear Research (Dubna, Russia) for providing HPC resources.

■ ABBREVIATIONS

FMF, familial Mediterranean fever; PAAND, pyrin-associated autoinflammation with neutrophilic dermatosis; MD, molecular dynamics

■ REFERENCES

(1) Munier, C. C.; Ottmann, C.; Perry, M. W. 14−3-3 Modulation of the Inflammatory Response. *Pharmacol. Res.* **2021**, *163*, 105236.

(2) Kastner, D. L. Hereditary Periodic Fever Syndromes. *Hematology Am. Soc. Hematol Educ Program* **2005**, 74−81.

(3) The International FMF Consortium. Ancient Missense Mutations in a New Member of the RoRet Gene Family Are Likely to Cause Familial Mediterranean Fever. *Cell* **1997**, *90* (4), 797−807.
(4) Arakelov, G.; Arakelov, V.; Nazaryan, K. Complex formation dynamics of native and mutated pyrin's B30.2 domain with caspase-1. *Proteins* **2018**, *86*, 676−683.
(5) Schnappauf, O.; Chae, J. J.; Kastner, D. L.; Aksentijevich, I. The Pyrin Inflammasome in Health and Disease Front. *Front. Immunol.* **2019**, *10*, 1745.
(6) Jéru, I.; Papin, S.; L'hoste, S.; Duquesnoy, P.; Cazeneuve, C.; Camonis, J.; Amselem, S. Interaction of Pyrin with 14.3.3 in an Isoform-Specific and Phosphorylation-Dependent Manner Regu-Lates Its Translocation to the Nucleus. *Arthritis Rheumatol.* **2005**, *52*, 1848−1857.
(7) Obsil, T.; Obsilova, V. Structural Basis of 14−3-3 Protein Functions Seminars in Cell &. *Dev. Biol.* **2011**, *22*, 663−672.
(8) Shimada, T.; Fournier, A. E.; Yamagata, K. 2013 Neuroprotec-Tive Function of 14−3-3 Proteins in Neurodegeneration. *Biomed. Res. Int.* **2013**, *2013*, 1−11.
(9) Shen, Y. H.; Godlewski, J.; Bronisz, A.; Zhu, J.; Comb, M. J.; Avruch, J.; Tzivion, G. Significance of 14−3-3 Self-Dimerization for Phosphorylation-Dependent Target Binding. *MboC* **2003**, *14*, 4721−4733.
(10) Fu, H.; Subramanian, R.; Masters, S. C. 14−3-3 Proteins: Structure, Function, and Regulation Annu. *Rev. Pharmacol. Toxicol.* **2000**, *40*, 617−647.
(11) Florian, R.; Gruber, P.; Hofmann, J.; Kirchmair, J. Modulators of Protein-Protein Interactions − Novel Approaches in Targeting Protein Kinases and Other Pharmaceutically Relevant Biomolecules. *Curr. Top. Med. Chem.* **2011**, *11*, 1305−1319.
(12) Thiel, P.; Kaiser, M.; Ottmann, C. Small-Molecule Stabilization of Protein-Protein Interactions: An Underestimated Concept in Drug Discovery? *Angew. Chem., Int. Ed.* **2012**, *51* (9), 2012−2018.
(13) Villoutreix, B. O.; Kuenemann, M. A.; Poyet, J. L.; Bruzzoni-Giovanelli, H.; Labbé, C.; Lagorce, D.; Sperandio, O.; Miteva, M. A. Drug-Like Protein—Protein Interaction Modulators: Challenges and Oppor-Tunities for Drug Discovery and Chemical Biology. *Mol. Inf.* **2014**, *33* (6−7), 414−437.
(14) Stanzione, F.; Giangreco, I.; Cole, J. C. Use of Molecular Docking Computational Tools in Drug Discovery. *Prog. Med. Chem.* **2021**, *60*, 273−343.
(15) Du, Z.; Su, H.; Wang, W.; Ye, L.; Wei, H.; Peng, Z.; Anishchenko, I.; Baker, D.; Yang, J. The trRosetta Server for Fast and Accu-Rate Protein Structure Prediction. *Nat. Protoc.* **2021**, *16*, 5634−5651.
(16) Totrov, M.; Abagyan, R. Detailed Ab Initio Prediction of Lysozyme-Antibody Complex with 1.6 Å Accuracy. *Nat. Struct. Biol.* **1994**, *1*, 259−263.
(17) Abagyan, R.; Totrov, M.; Kuznetsov, D. C. ICM—a New Method for Protein Modeling and Design: Applications to Docking and Structure Prediction from the Distorted Native Con-Formation. *J. Comput. Chem.* **1994**, *15* (5), 488−506.
(18) Case, D.; Ben-Shalom, I.; Brozell, S.; Cerutti, D.; Cheatham, T., III; Cruzeiro, V.; Darden, T.; Duke, R.; Ghoreishi, D.; Gilson, M. *AMBER 2018*. University of California, San Fran-Cisco, 2018.
(19) Wang, J.; Wolf, R. M.; Caldwell, J. W.; Kollman, P. A.; Case, D. A. Development and Testing of a General Amber Force Field. *J. Comput. Chem.* **2004**, *25* (9), 1157−1174.
(20) Roe, D. R.; Cheatham, T. E. PTRAJ and CPPTRAJ: Soft-Ware for Processing and Analysis of Molecular Dynamics Tra-Jectory Data. *J. Chem. Theory Comput.* **2013**, *9*, 3084−3095.
(21) Tubiana, T.; Carvaillo, J. C.; Boulard, Y. S.; Bressanelli, C. TTClust: A Versatile Molecular Simulation Trajectory Clustering Program with Graphical Summaries. *J. Chem. Inf. Model.* **2018**, *58* (11), 2178−2182.
(22) Case, D. A.; Aktulga, H. M.; Belfon, K.; Ben-Shalom, I. Y.; Berryman, J. T.; Brozell, S. R.; Cerutti, D. S.; Cheatham, T. E., III; Cisneros, G. A.; Cruzeiro, V. W. D. *Amber 2023*; University of Cali-Fornia: San Francisco, 2023
(23) Djoumbou Feunang, Y.; Eisner, R.; Knox, C.; Chepelev, L.; Hastings, J.; Owen, G.; Fahy, E.; Steinbeck, C.; Subramanian, S.; Bolton, E.; et al. ClassyFire: Automated Chemi-Cal Classification with a Comprehensive. *J. Cheminform.* **2016**, *8*, 1−20.
(24) Daina, A.; Michielin, O.; Zoete, V. SwissADME: A Free Web Tool to Evaluate Pharmacokinetics, Drug-Likeness and Me-Dicinal Chemistry Friendliness of Small Molecules. *Sci. Rep.* **2017**, *7*, 42717.
(25) BIOVIA, Dassault Systèmes. *Discovery Studio Visualizer, V21.1.0.20298; Release 2020*. Dassault Systèmes, San Diego, CA, USA, 2021.https://Discover.3ds.Com/Discovery-Studio-Visualizer-Download.
(26) Prasanna, S.; Doerksen, R. Topological Polar Surface Area: A Useful Descriptor in 2D-QSAR. *Curr. Med. Chem.* **2009**, *16*, 21−41.
(27) Padrón, J. A.; Carrasco, R.; Pellón, R. F. Molecular Descriptor Based on a Molar Refractivity Partition Using Randic-Type Graph-Theoretical Invariant. *J. Pharm. Pharmaceut. Sci.* **2002**, *5* (3), 258−266.
(28) Veber, D. F.; Johnson, S. R.; Cheng, H.-Y.; Smith, B. R.; Ward, K. W.; Kopple, K. D. Molecular Properties That Influence the Oral Bioavailability of Drug Candidates J. *Med. Chem.* **2002**, *45*, 2615−2623.
(29) Pathania, S.; Singh, P. K. Analyzing FDA-Approved Drugs for Compliance of Pharmacokinetic Principles: Should There Be a Critical Screening Parameter in Drug Designing Protocols? *Expert Opin. Drug Metab. Toxicol.* **2021**, *17*, 351−354.
(30) Rehman, A. U.; Khurshid, B.; Ali, Y.; Rasheed, S.; Wadood, A.; Ng, H. L.; Chen, H. F.; Wei, Z.; Luo, R.; Zhang, J. Computational Approaches for the Design of Modulators Targeting Protein-Protein Interactions. *Expert Opin. Drug Discovery* **2023**, *18* (3), 315−333.
(31) Tovar, C.; Rosinski, J.; Filipovic, Z.; Higgins, B.; Kolinsky, K.; Hilton, H.; Zhao, X.; Vu, B. T.; Qing, W.; Packman, K.; Myklebost, O.; Heimbrook, D. C.; Vassilev, L. T. Small-Molecule MDM2 Antagonists Reveal Aberrant P53 Signaling in Cancer: Implications for Therapy. *Proc. Natl. Acad. Sci. U. S. A.* **2006**, *103* (6), 1888−1893.
(32) Vassilev, L. T.; Vu, B. T.; Graves, B.; Carvajal, D.; Podlaski, F.; Filipovic, Z.; Kong, N.; Kammlott, U.; Lukacs, C.; Klein, C.; Fotouhi, N.; Liu, E. A. In Vivo Activation of the P53 Pathway by Small-Molecule Antagonists of MDM2. *Science* **2004**, *303* (5659), 844−848.
(33) Tse, C.; Shoemaker, A. R.; Adickes, J.; Anderson, M. G.; Chen, J.; Jin, S.; Johnson, E. F.; Marsh, K. C.; Mitten, M. J.; Nimmer, P.; Roberts, L.; Tahir, S. K.; Xiao, Y.; Yang, X.; Zhang, H.; Fesik, S.; Rosenberg, S. H.; Elmore, S. W. ABT-263: A Potent and Orally Bioavailable Bcl-2 Family Inhibitor. *Cancer Res.* **2008**, *68* (9), 3421−3428.
(34) Oltersdorf, T.; Elmore, S. W.; Shoemaker, A. R.; Armstrong, R. C.; Augeri, D. J.; Belli, B. A.; Bruncko, M.; Deckwerth, T. L.; Dinges, J.; Hajduk, P. J.; Joseph, M. K.; Kitada, S.; Korsmeyer, S. J.; Kunzer, A. R.; Letai, A.; Li, C.; Mitten, M. J.; Nettesheim, D. G.; Ng, S.; Nimmer, P. M.; O'Connor, J. M.; Oleksijew, A.; Petros, A. M.; Reed, J. C.; Shen, W.; Tahir, S. K.; Thompson, C. B.; Tomaselli, K. J.; Wang, B.; Wendt, M. D.; Zhang, H.; Fesik, S. W.; Rosenberg, S. H. An Inhibitor of Bcl-2 Family Proteins Induces Regression of Solid Tumours. *Nature* **2005**, *435* (7042), 677−681.
(35) Lau, R.; Hann, M. M.; Ottmann, C. Crystal Structure and Ligandability of the 14−3-3/Pyrin Interface. *Biochem. Biophys. Res. Commun.* **2023**, *651*, 1−7.

https://doi.org/10.1021/acsomega.4c07386
ACS Omega 2025, 10, 3462−3473